ELSEVIER

SCIENCE DIRECT

Physics Letters B 602 (2004) 167–179

PHYSICS LETTERS B

www.elsevier.com/locate/physletb

Multi-photon events with large missing energy in e^+e^- collisions at $\sqrt{s} = 192$–209 GeV

OPAL Collaboration

G. Abbiendi [b], C. Ainsley [e], P.F. Åkesson [c,22], G. Alexander [u], J. Allison [o], P. Amaral [h], G. Anagnostou [a], K.J. Anderson [h], S. Arcelli [b], S. Asai [v,w], D. Axen [aa], G. Azuelos [q,1], I. Bailey [z], E. Barberio [g,14], T. Barillari [af], R.J. Barlow [o], R.J. Batley [e], P. Bechtle [y], T. Behnke [y], K.W. Bell [s], P.J. Bell [a], G. Bella [u], A. Bellerive [f], G. Benelli [d], S. Bethke [af], O. Biebel [ae], O. Boeriu [i], P. Bock [j], M. Boutemeur [ae], S. Braibant [g], L. Brigliadori [b], R.M. Brown [s], K. Buesser [y], H.J. Burckhart [g], S. Campana [d], R.K. Carnegie [f], A.A. Carter [l], J.R. Carter [e], C.Y. Chang [p], D.G. Charlton [a], C. Ciocca [b], A. Csilling [ac], M. Cuffiani [b], S. Dado [t], A. De Roeck [g], E.A. De Wolf [g,17], K. Desch [y], B. Dienes [ad], M. Donkers [f], J. Dubbert [ae], E. Duchovni [x], G. Duckeck [ae], I.P. Duerdoth [o], E. Etzion [u], F. Fabbri [b], L. Feld [i], P. Ferrari [g], F. Fiedler [ae], I. Fleck [i], M. Ford [e], A. Frey [g], P. Gagnon [k], J.W. Gary [d], G. Gaycken [y], C. Geich-Gimbel [c], G. Giacomelli [b], P. Giacomelli [b], M. Giunta [d], J. Goldberg [t], E. Gross [x], J. Grunhaus [u], M. Gruwé [g], P.O. Günther [c], A. Gupta [h], C. Hajdu [ac], M. Hamann [y], G.G. Hanson [d], A. Harel [t], M. Hauschild [g], C.M. Hawkes [a], R. Hawkings [g], R.J. Hemingway [f], G. Herten [i], R.D. Heuer [y], J.C. Hill [e], K. Hoffman [h], D. Horváth [ac,2], P. Igo-Kemenes [j], K. Ishii [v,w], H. Jeremie [q], P. Jovanovic [a], T.R. Junk [f,7], N. Kanaya [z], J. Kanzaki [v,w,18], D. Karlen [z], K. Kawagoe [v,w], T. Kawamoto [v,w], R.K. Keeler [z], R.G. Kellogg [p], B.W. Kennedy [s], S. Kluth [af], T. Kobayashi [v,w], M. Kobel [c], S. Komamiya [v,w], T. Krämer [y], P. Krieger [f,10], J. von Krogh [j], K. Kruger [g], T. Kuhl [y], M. Kupper [x], G.D. Lafferty [o], H. Landsman [t], D. Lanske [m], J.G. Layter [d], D. Lellouch [x], J. Letts [13], L. Levinson [x], J. Lillich [i], S.L. Lloyd [l], F.K. Loebinger [o], J. Lu [aa,20], A. Ludwig [c], J. Ludwig [i], W. Mader [c], S. Marcellini [b], A.J. Martin [l], G. Masetti [b], T. Mashimo [v,w], P. Mättig [11], J. McKenna [aa], R.A. McPherson [z], F. Meijers [g], W. Menges [y], F.S. Merritt [h], H. Mes [f,1], N. Meyer [y], A. Michelini [b], S. Mihara [v,w], G. Mikenberg [x], D.J. Miller [n], S. Moed [t], W. Mohr [i], T. Mori [v,w], A. Mutter [i], K. Nagai [l], I. Nakamura [v,w,19], H. Nanjo [v,w], H.A. Neal [ag], R. Nisius [af], S.W. O'Neale [a,✠], A. Oh [g], M.J. Oreglia [h], S. Orito [v,w,✠], C. Pahl [af],

doi:10.1016/j.physletb.2004.09.059

G. Pásztor [d,5], J.R. Pater [o], J.E. Pilcher [h], J. Pinfold [ab], D.E. Plane [g], B. Poli [b], O. Pooth [m], M. Przybycień [g,12], A. Quadt [c], K. Rabbertz [g,16], C. Rembser [g], P. Renkel [x], J.M. Roney [z], Y. Rozen [t], K. Runge [i], K. Sachs [f], T. Saeki [v,w], E.K.G. Sarkisyan [g,8], A.D. Schaile [ae], O. Schaile [ae], P. Scharff-Hansen [g], J. Schieck [af], T. Schörner-Sadenius [g,23], M. Schröder [g], M. Schumacher [c], W.G. Scott [s], R. Seuster [m,4], T.G. Shears [g,6], B.C. Shen [d], P. Sherwood [n], A. Skuja [p], A.M. Smith [g], R. Sobie [z], S. Söldner-Rembold [n], F. Spano [h], A. Stahl [c,21], D. Strom [r], R. Ströhmer [ae], S. Tarem [t], M. Tasevsky [g,17], R. Teuscher [h], M.A. Thomson [e], E. Torrence [r], D. Toya [v,w], P. Tran [d], I. Trigger [g], Z. Trócsányi [ad,3], E. Tsur [u], M.F. Turner-Watson [a], I. Ueda [v,w], B. Ujvári [ad,3], C.F. Vollmer [ae], P. Vannerem [i], R. Vértesi [ad,3], M. Verzocchi [p], H. Voss [g,15], J. Vossebeld [g,6], C.P. Ward [e], D.R. Ward [e], P.M. Watkins [a], A.T. Watson [a], N.K. Watson [a], P.S. Wells [g], T. Wengler [g], N. Wermes [c], G.W. Wilson [o,9], J.A. Wilson [a], G. Wolf [x], T.R. Wyatt [o], S. Yamashita [v,w], D. Zer-Zion [d], L. Zivkovic [x]

[a] *School of Physics and Astronomy, University of Birmingham, Birmingham B15 2TT, UK*
[b] *Dipartimento di Fisica dell'Università di Bologna and INFN, I-40126 Bologna, Italy*
[c] *Physikalisches Institut, Universität Bonn, D-53115 Bonn, Germany*
[d] *Department of Physics, University of California, Riverside, CA 92521, USA*
[e] *Cavendish Laboratory, Cambridge CB3 0HE, UK*
[f] *Ottawa-Carleton Institute for Physics, Department of Physics, Carleton University, Ottawa, Ontario K1S 5B6, Canada*
[g] *CERN, European Organisation for Nuclear Research, CH-1211 Geneva 23, Switzerland*
[h] *Enrico Fermi Institute and Department of Physics, University of Chicago, Chicago, IL 60637, USA*
[i] *Fakultät für Physik, Albert-Ludwigs-Universität Freiburg, D-79104 Freiburg, Germany*
[j] *Physikalisches Institut, Universität Heidelberg, D-69120 Heidelberg, Germany*
[k] *Indiana University, Department of Physics, Bloomington, IN 47405, USA*
[l] *Queen Mary and Westfield College, University of London, London E1 4NS, UK*
[m] *Technische Hochschule Aachen, III Physikalisches Institut, Sommerfeldstrasse 26-28, D-52056 Aachen, Germany*
[n] *University College London, London WC1E 6BT, UK*
[o] *Department of Physics, Schuster Laboratory, The University, Manchester M13 9PL, UK*
[p] *Department of Physics, University of Maryland, College Park, MD 20742, USA*
[q] *Laboratoire de Physique Nucléaire, Université de Montréal, Montréal, Québec H3C 3J7, Canada*
[r] *University of Oregon, Department of Physics, Eugene, OR 97403, USA*
[s] *CCLRC Rutherford Appleton Laboratory, Chilton, Didcot, Oxfordshire OX11 0QX, UK*
[t] *Department of Physics, Technion-Israel Institute of Technology, Haifa 32000, Israel*
[u] *Department of Physics and Astronomy, Tel Aviv University, Tel Aviv 69978, Israel*
[v] *International Centre for Elementary Particle Physics and Department of Physics, University of Tokyo, Tokyo 113-0033, Japan*
[w] *Kobe University, Kobe 657-8501, Japan*
[x] *Particle Physics Department, Weizmann Institute of Science, Rehovot 76100, Israel*
[y] *Universität Hamburg/DESY, Institut für Experimentalphysik, Notkestrasse 85, D-22607 Hamburg, Germany*
[z] *University of Victoria, Department of Physics, PO Box 3055, Victoria BC V8W 3P6, Canada*
[aa] *University of British Columbia, Department of Physics, Vancouver BC V6T 1Z1, Canada*
[ab] *University of Alberta, Department of Physics, Edmonton AB T6G 2J1, Canada*
[ac] *Research Institute for Particle and Nuclear Physics, H-1525 Budapest, PO Box 49, Hungary*
[ad] *Institute of Nuclear Research, H-4001 Debrecen, PO Box 51, Hungary*
[ae] *Ludwig-Maximilians-Universität München, Sektion Physik, Am Coulombwall 1, D-85748 Garching, Germany*
[af] *Max-Planck-Institute für Physik, Föhringer Ring 6, D-80805 München, Germany*
[ag] *Yale University, Department of Physics, New Haven, CT 06520, USA*

Received 14 July 2004; received in revised form 13 September 2004; accepted 19 September 2004

Available online 12 October 2004

Editor: L. Rolandi

Abstract

Events with a final state consisting of two or more photons and large missing transverse energy have been observed in e^+e^- collisions at centre-of-mass energies in the range 192–209 GeV using the OPAL detector at LEP. Cross-section measurements are performed within the kinematic acceptance of the selection and compared with the expectations from the Standard Model process $e^+e^- \to \nu\bar{\nu}\gamma\gamma(\gamma)$. No evidence for new physics contributions to this final state is observed. Upper limits on $\sigma(e^+e^- \to XX) \cdot BR^2(X \to Y\gamma)$ are derived for the case of stable and invisible Y. In the case of massive Y the combined limits obtained from all the data range from 10 to 60 fb, while for the special case of massless Y the range is 20 to 40 fb. The limits apply to pair production of excited neutrinos ($X = \nu^*, Y = \nu$), to neutralino production ($X = \tilde{\chi}_2^0, Y = \tilde{\chi}_1^0$) and to supersymmetric models in which $X = \tilde{\chi}_1^0$ and $Y = \tilde{G}$ is a light gravitino.

1. Introduction

We describe measurements and searches performed using a data sample of photonic events with large missing transverse energy collected with the OPAL detector in 1999 and 2000, the final two years of LEP operation. The events result from e^+e^- collisions in the centre-of-mass energy range of about 192–209 GeV with a combined integrated luminosity of 426.5 pb^{-1}. When deriving cross-section limits on new physics processes, these data are combined with previously published data [1] taken at 189 GeV and corresponding to 177.3 pb^{-1}. The present Letter builds on past publications based on data samples collected at lower centre-of-mass energies [1–3]. The new data samples, taken at the highest energies achieved by LEP, provide discovery potential in a new kinematic regime with a large increase in integrated luminosity. Similar searches have been made by the other LEP Collaborations [4].

The analysis presented here is designed to select events with two photons and significant missing transverse energy in the final state, indicating the presence of at least one neutrino-like invisible particle which interacts only weakly with matter. The event selection for this search topology, identical to that used in our most recent publication [1], is designed to retain acceptance for events with an additional photon, provided that the system formed by the three photons is consistent with the presence of significant missing transverse energy. Within the Standard Model, such events are expected from the $e^+e^- \to \nu\bar{\nu}\gamma\gamma(\gamma)$ process.

This final-state topology is also sensitive to several new physics scenarios. In the context of the search for new physics, the emphasis in this publication is on general searches applicable to a broad class of models. To this end, a generic classification is used: $e^+e^- \to XX$ where X is neutral and can decay radia-

E-mail address: plane@cern.ch (D.E. Plane).
[1] And at TRIUMF, Vancouver, Canada V6T 2A3.
[2] And Institute of Nuclear Research, Debrecen, Hungary.
[3] And Department of Experimental Physics, University of Debrecen, Hungary.
[4] And MPI München.
[5] And Research Institute for Particle and Nuclear Physics, Budapest, Hungary.
[6] Now at University of Liverpool, Department of Physics, Liverpool L69 3BX, UK.
[7] Now at Department of Physics, University of Illinois at Urbana-Champaign, USA.
[8] And Manchester University.
[9] Now at University of Kansas, Department of Physics and Astronomy, Lawrence, KS 66045, USA.
[10] Now at University of Toronto, Department of Physics, Toronto, Canada.
[11] Current address Bergische Universität, Wuppertal, Germany.
[12] Now at University of Mining and Metallurgy, Cracow, Poland.
[13] Now at University of California, San Diego, USA.
[14] Now at The University of Melbourne, Victoria, Australia.
[15] Now at IPHE Université de Lausanne, CH-1015 Lausanne, Switzerland.
[16] Now at IEKP Universität Karlsruhe, Germany.
[17] Now at University of Antwerpen, Physics Department, B-2610 Antwerpen, Belgium; supported by Interuniversity Attraction Poles Programme—Belgian Science Policy.
[18] And High Energy Accelerator Research Organisation (KEK), Tsukuba, Ibaraki, Japan.
[19] Now at University of Pennsylvania, Philadelphia, PA, USA.
[20] Now at TRIUMF, Vancouver, Canada.
[21] Now at DESY Zeuthen.
[22] Now at CERN.
[23] Now at DESY.
✠ Deceased.

tively ($X \to Y\gamma$) and Y is stable and only weakly interacting. The limits presented for this generic process are applicable to a variety of physics searches. For the general case of massive X and Y this includes conventional supersymmetric processes ($X = \tilde{\chi}_2^0, Y = \tilde{\chi}_1^0$). There is particularly good sensitivity for the special case of $M_Y \approx 0$. This is applicable both to the production of excited neutrinos ($X = \nu^*, Y = \nu$) and to supersymmetric models in which the lightest supersymmetric particle (LSP) is a light gravitino and $\tilde{\chi}_1^0$ is the next-to-lightest supersymmetric particle (NLSP) which decays to a gravitino and a photon ($X = \tilde{\chi}_1^0, Y = \tilde{G}$). In the latter case, we also set limits on an example light-gravitino model [5]. The neutralino lifetime in such models is a free parameter. In this Letter we address only the case of promptly decaying X.

This search topology also has sensitivity to the production of two particles, one invisible, or with an invisible decay mode, and the other decaying into two photons. Such events might arise from the production of a Higgs-like scalar particle, S^0: $e^+e^- \to Z^0S^0$, followed by $S^0 \to \gamma\gamma$, $Z^0 \to \nu\bar{\nu}$. The results of an OPAL search for this process, including the hadronic and leptonic Z^0 decays, have been separately reported [6]. Finally, this search topology can also probe $WW\gamma\gamma$ quartic couplings in the $e^+e^- \to \nu_e\overline{\nu_e}\gamma\gamma$ process. The OPAL quartic gauge coupling measurements are described in [7].

This Letter first describes the OPAL detector and the Monte Carlo samples used. A brief summary of the event selection will then be given, followed by cross-section measurements and comparisons with Standard Model expectations. The new physics search results will then be discussed.

2. OPAL detector and Monte Carlo samples

The OPAL detector, which is described in detail in [8], contained a silicon micro-vertex detector surrounded by a pressurized central tracking system operating inside a solenoid with a magnetic field of 0.435 T. The barrel and endcap regions of the detector were instrumented with scintillation counters, presamplers and a lead-glass electromagnetic calorimeter (ECAL). The magnet return yoke was instrumented for hadron calorimetry and was surrounded by muon chambers. Electromagnetic calorimeters close to the beam axis measured luminosity and completed the acceptance.

The measurements presented here are based mainly on the observation of clusters of energy deposited in the lead-glass electromagnetic calorimeter. This consisted of an array of 9440 lead-glass blocks in the barrel region, $|\cos\theta| < 0.82$, with a quasi-pointing geometry and two endcap arrays, each of 1132 lead-glass blocks, covering the polar angle[24] range, $0.81 < |\cos\theta| < 0.984$. Hermetic electromagnetic calorimeter coverage was achieved beyond the end of the ECAL down to 33 mrad in polar angle with the use of the gamma-catcher calorimeter, the forward calorimeter and the silicon-tungsten calorimeter.

Scintillators in the barrel and endcap regions were used to reject backgrounds from cosmic-ray interactions by providing time measurements for the large fraction ($\approx 80\%$) of photons which converted in the material in front of the ECAL. The barrel time-of-flight (TOF) scintillator bars were located outside the solenoid in front of the barrel ECAL and matched its geometrical acceptance $|\cos\theta| < 0.82$. Tile endcap (TE) scintillator arrays were located in front of the endcap ECAL at $0.81 < |\cos\theta| < 0.955$. Additional scintillating-tile arrays, referred to as the MIP plug, were located at more forward angles. In the region from 125 to 200 mrad these detectors were used to provide redundancy in the rejection of events with significant electromagnetic activity in the forward region.

The integrated luminosities of the data samples are determined to better than 1% from small-angle Bhabha scattering events in the silicon-tungsten calorimeter. Triggers based on electromagnetic energy deposits in either the barrel or endcap electromagnetic calorimeters lead to full trigger efficiency for photonic events passing the event selection criteria used in this analysis.

The NUNUGPV98 [9] and KK2f [10] Monte Carlo generators were used to simulate the Standard Model signal process, $e^+e^- \to \nu\bar{\nu}\gamma\gamma(\gamma)$. For other expected Standard Model processes, a number

[24] The OPAL right-handed coordinate system is defined such that the origin is at the centre of the detector and the z axis points along the direction of the e^- beam. The polar angle θ is defined with respect to the e^- beam direction and ϕ is the azimuthal angle measured from the $+x$ axis.

of different generators were used: RADCOR [11] for $e^+e^- \to \gamma\gamma(\gamma)$; BHWIDE [12] and TEEGG [13] for $e^+e^- \to e^+e^-(\gamma)$; KORALW [14] using `grc4f` [15] matrix elements for $e^+e^- \to \nu\bar{\nu}\ell^+\ell^-(\gamma)$ and $e^+e^- \to \nu\bar{\nu}q\bar{q}(\gamma)$, and KORALZ [16] for $e^+e^- \to \mu^+\mu^-(\gamma)$ and $e^+e^- \to \tau^+\tau^-(\gamma)$. The BDK program [17] was used for $e^+e^- \to e^+e^-\ell^+\ell^-$, except for $e^+e^- \to e^+e^-e^+e^-$ which was generated using the Vermaseren program [18]. The expected contribution from each of these Standard Model processes was evaluated using a total equivalent integrated luminosity at least five times larger than the integrated luminosity of the data sample.

To simulate possible new physics processes of the type $e^+e^- \to XX$ where X decays to $Y\gamma$ and Y escapes detection, a modified version of the SUSYGEN [19] Monte Carlo generator was used to produce neutralino pair events of the type $e^+e^- \to \tilde{\chi}_2^0\tilde{\chi}_2^0$, $\tilde{\chi}_2^0 \to \tilde{\chi}_1^0\gamma$, with isotropic angular distributions for the production and decay of $\tilde{\chi}_2^0$ and including the effects of initial-state radiation. For $\sqrt{s} = 206$ GeV, Monte Carlo events were generated at 49 points in the kinematically accessible region of the (M_X, M_Y) plane. Monte Carlo events at 42 points in (M_X, M_Y) with $\sqrt{s} = 189$ GeV were generated for our previous publication [1]. Using these two samples, the selection efficiency was determined for each generated point and then parametrized as a function of (M_X, M_Y) and centre-of-mass energy. The efficiency varies slowly with energy and for energies above 206 GeV, the 206 GeV values were used. All Monte Carlo samples described above were processed through the full OPAL detector simulation [20].

3. Event selection

A detailed description of the event selection is given in our previous publications [1,2]. In brief, photons are identified as energy deposits in the electromagnetic calorimeter. Events are required to have no other significant activity, except for the possibility of additional photons. Information from the tracking chambers is used to reject electromagnetic clusters associated with prompt charged tracks while retaining sensitivity for photons which converted in the material between the interaction point and the calorimeter. Timing information is used to reject backgrounds from cosmic-ray events. Events with activity beyond the acceptance of the ECAL are vetoed using information from the gamma catcher, the forward calorimeter, the silicon-tungsten calorimeter and the MIP plug. The kinematic acceptance of the selection is defined by requiring:

- at least two photons, each with $x_\gamma > 0.05$ and $15^\circ < \theta < 165^\circ$, or one photon with $E_\gamma > 1.75$ GeV and $|\cos\theta| < 0.8$ and a second photon with $E_\gamma > 1.75$ GeV and $15^\circ < \theta < 165^\circ$; here E_γ is the photon energy, θ is the photon polar angle and x_γ is the photon scaled energy $E_\gamma/E_{\mathrm{beam}}$;
- that the two-photon system consisting of the two highest-energy photons have momentum transverse to the beamline $(p_T^{\gamma\gamma})$ satisfying $p_T^{\gamma\gamma}/E_{\mathrm{beam}} > 0.05$.

The selection is designed to retain acceptance for events with additional photons in which the resulting photonic system is still consistent with the presence of significant missing energy. This reduces the sensitivity of the measurement to the modelling of higher-order contributions.

4. Selection results

The data described in this Letter were taken during the final two years of LEP operation, at centre-of-mass energies between 192 and 209 GeV. For the purposes of this publication the data have been binned into six samples with mean centre-of-mass energies of approximately 192, 196, 200, 202, 205 and 207 GeV. The energy ranges and luminosity breakdown are summarized in Table 1. Applied to the entire sample, the selection yields a total of 54 events, in good agreement with the KK2f prediction of 57.2 ± 1.3 events for the Standard Model $e^+e^- \to \nu\bar{\nu}\gamma\gamma(\gamma)$ contribution. The expected contribution from other Standard Model processes and from cosmic ray and beam-related backgrounds is 1.2 ± 0.3 events, dominated by contributions from low-angle radiative Bhabha events and radiative four-fermion final states. The selection results are included in Table 1. The selection efficiency for $e^+e^- \to \nu\bar{\nu}\gamma\gamma(\gamma)$ events within the kinematic acceptance of the selection is $(65.7 \pm 1.5)\%$, independent

Table 1
Results of the selection applied to the OPAL 1999 and 2000 data samples. Shown for each subsample are the integrated luminosity $\mathcal{L}$, the centre-of-mass energy range, the luminosity-weighted mean centre-of-mass energy, the numbers of events observed and expected, and the measured and predicted cross-section for the process $e^+e^- \to \nu\bar{\nu}\gamma\gamma(\gamma)$, within the kinematic acceptance of the selection. Predicted values were obtained using the KK2f Monte Carlo generator. The errors shown are the sum of the statistical and systematic uncertainties

Sample	$\mathcal{L}$ (pb^{-1})	$\sqrt{s}$ (GeV)	$\langle\sqrt{s}\rangle$	$N_{\rm obs}$	$N_{\rm exp}^{\nu\bar{\nu}\gamma\gamma(\gamma)}$	$\sigma_{\rm meas}^{\nu\bar{\nu}\gamma\gamma(\gamma)}$ (pb)	$\sigma_{\rm KK2f}^{\nu\bar{\nu}\gamma\gamma(\gamma)}$ (pb)
192	28.9	190–194	191.6	4	4.26 ± 0.11	0.21 ± 0.10	0.222 ± 0.003
196	72.3	194–198	195.6	5	9.97 ± 0.25	0.11 ± 0.05	0.215 ± 0.002
200	74.8	198–201	199.5	14	10.10 ± 0.25	0.29 ± 0.08	0.207 ± 0.001
202	39.2	201–203	201.7	6	5.21 ± 0.14	0.23 ± 0.10	0.203 ± 0.002
205	79.1	203–206	205.0	10	10.34 ± 0.26	0.19 ± 0.06	0.198 ± 0.001
207	132.2	206–209	206.6	15	17.28 ± 0.43	0.17 ± 0.04	0.196 ± 0.001

of energy. The cross-section within the kinematic acceptance of the selection is also shown in Table 1 as are the corresponding predictions obtained using the KK2f Monte Carlo generator. The predictions of the NUNUGPV98 Monte Carlo generator were also examined and agreed well with those of KK2f. Small differences are accounted for in the systematic uncertainties.

The dominant sources of systematic uncertainties arise from modelling of the event selection efficiency, especially the simulation of the detector material and consequent photon conversion probabilities. The effects of these uncertainties and of uncertainties on the efficiency of timing cuts used to suppress cosmic-ray events are calculated accounting for different event topologies (both photons in the barrel region, both in the endcap, or one in each). This total uncertainty is 1.7%. Other sources arise from uncertainties on the integrated luminosity measurement (0.5%), on detector occupancy estimates (1%) obtained from the analysis of randomly triggered events, on comparisons of different Monte Carlo event generators for the process $e^+e^- \to \nu\bar{\nu}\gamma\gamma(\gamma)$ (1%). The total systematic uncertainty common to each energy bin is 2.3%. In individual energy bins, Monte Carlo statistics account for an additional systematic uncertainty of 0.9–1.4%.

The kinematic properties of the selected events, summed over all energies, are displayed in Fig. 1 where they are compared with the predicted distributions for $e^+e^- \to \nu\bar{\nu}\gamma\gamma(\gamma)$ obtained using the KK2f generator normalized to the integrated luminosity of the data. Plot (a) shows the recoil mass distribution of the selected events (for the two most energetic photons in the case of events with three or more photons). The distribution is peaked near the mass of the Z^0 as is expected for contributions from $e^+e^- \to \nu\bar{\nu}\gamma\gamma(\gamma)$. The resolution of the recoil mass is typically 4–6 GeV for $M_{\rm recoil} \approx M_Z$. Events with a negative recoil-mass squared are plotted in the zero bin of the distribution. Plot (b) shows the distribution of the scaled energy of the second most energetic photon. Plot (c) shows the $\gamma\gamma$ invariant-mass distribution for which the mass resolution is typically 1–2 GeV. Plot (d) shows the distribution in scaled transverse momentum of the selected two-photon system.

There are 3 selected events having a third photon with deposited energy above 300 MeV and within the polar-angle acceptance of the selection. The corresponding expectation from KK2f is 3.36 ± 0.08 events.

5. Data interpretation

The results of this selection are used to test the Standard Model and to search for new physics contributions. In the absence of an excess of events beyond the Standard Model expectation, we set 95% CL upper limits on the quantity $\sigma(e^+e^- \to XX) \cdot BR^2(X \to Y\gamma)$ for the general case of massive X and Y, and separately for the special case of $M_Y \approx 0$. Efficiencies were evaluated under the assumption that X decays promptly. Monte Carlo samples were generated for a variety of mass points in the kinematically accessible region of the (M_X, M_Y) plane. To set limits for arbitrary M_X and M_Y, the efficiency over the entire (M_X, M_Y) plane was parameterized using the efficiencies calculated at the generated mass points. For M_X values below $M_Z/2$, search results based on LEP1 data have been previously reported [21]. In this low-mass region, events with radiative return to the Z^0 followed

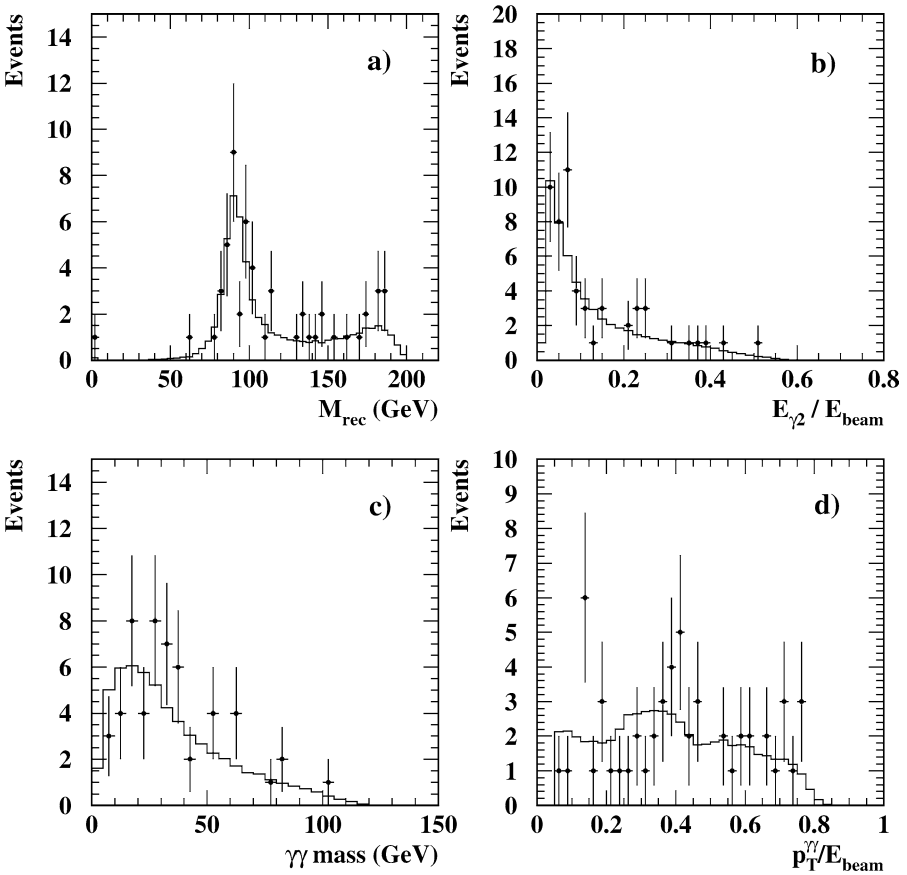

Fig. 1. Kinematic quantities of selected multi-photon events. Shown are (a) the recoil-mass distribution, (b) the distribution of the scaled energy of the second photon, (c) the distribution of the invariant mass of the $\gamma\gamma$ system, and (d) the scaled transverse momentum distribution for the $\gamma\gamma$ system. The data points with error bars represent the selected OPAL data events. In each case the histogram shows the expected contribution from $e^+e^- \to \nu\bar{\nu}\gamma\gamma(\gamma)$ events, from KK2f, normalized to the integrated luminosity of the data. The expected background from other sources (1.2 ± 0.3 events) is not shown.

by $Z^0 \to XX$ would yield very different kinematics than those used here to generate the signal Monte Carlo samples. For this reason, the search is restricted to the mass region $M_X > M_Z/2$.

5.1. *Search for* $e^+e^- \to XX$, $X \to Y\gamma$*; general case:* $M_Y \geqslant 0$

The searches for $e^+e^- \to XX$, $X \to Y\gamma$, both for the general case discussed here and the special case of $M_Y \approx 0$ discussed in Section 5.2, use the methods described in our previous publications [1,2]. Selected events are classified as consistent with a given value of M_X and M_Y if the energy of each of the photons falls within the region kinematically accessible to photons from the process $e^+e^- \to XX$, $X \to Y\gamma$, including resolution effects. Selection efficiencies at some of the generated grid points for the $e^+e^- \to XX$, $X \to Y\gamma$ $\sqrt{s} = 206$ GeV Monte Carlo events are shown in Table 2. These values include the efficiency of the kinematic consistency requirement which is higher than 95% at each generated point in the region of the (M_X, M_Y) plane. For $M_X - M_Y$ values lower than 5 GeV the efficiency begins to fall off rapidly and is thus difficult to model accurately. For this reason, we place limits only in the region of the (M_X, M_Y) plane satisfying $M_X - M_Y \geqslant 5$ GeV. Efficiencies at lower centre-of-mass energies are obtained from an interpolation between these efficiencies and the equivalent efficiencies at 189 GeV, which are given in our pre-

Table 2
Selection efficiencies (%) for the process $e^+e^- \to XX$, $X \to Y\gamma$ at $\sqrt{s} = 206$ GeV for various M_X and M_Y (GeV), after application of kinematic-consistency cuts. Not shown are the values for $M_Y = 20$ GeV, $M_Y = M_X - 15$ GeV and $M_Y = M_X - 2.5$ GeV. The errors shown are due to Monte Carlo statistics only

M_X (GeV)	$M_Y = 0$	$M_Y = M_X/2$	$M_Y = M_X - 10$	$M_Y = M_X - 5$
102.5	74.5 ± 1.2	74.7 ± 1.1	63.2 ± 1.3	33.8 ± 1.5
100	74.5 ± 1.2	74.4 ± 1.1	61.4 ± 1.3	32.3 ± 1.5
90	74.3 ± 1.2	75.1 ± 1.1	60.4 ± 1.4	36.2 ± 1.5
80	73.2 ± 1.2	73.5 ± 1.2	65.4 ± 1.3	37.8 ± 1.5
70	74.1 ± 1.2	71.7 ± 1.2	62.0 ± 1.4	39.0 ± 1.5
60	73.8 ± 1.1	71.5 ± 1.2	62.5 ± 1.4	41.2 ± 1.5
50	72.1 ± 1.2	71.5 ± 1.2	65.2 ± 1.3	43.5 ± 1.5

vious publication [1]. For data taken at centre-of-mass energies above 206 GeV, the 206 GeV efficiencies are used.

Events from $e^+e^- \to \nu\bar{\nu}\gamma\gamma(\gamma)$ are typically characterized by a high-energy photon from the radiative return to the Z^0 and a second lower energy photon. The kinematic consistency requirement is such that the two photons must have energies within the same (kinematically accessible) region. Thus, as M_X and M_Y increase, the allowed range of energy for the photons narrows, and fewer $\nu\bar{\nu}\gamma\gamma(\gamma)$ events will be accepted. For the 54 selected events, the distribution of the number of events consistent with a given mass point (M_X, M_Y) is consistent with the expectation from $e^+e^- \to \nu\bar{\nu}\gamma\gamma(\gamma)$ Monte Carlo, over the full (M_X, M_Y) plane. Upper limits are placed on $\sigma(e^+e^- \to XX) \cdot BR^2(X \to Y\gamma)$ accounting for the number of selected events and the expected number of background events from the process $e^+e^- \to \nu\bar{\nu}\gamma\gamma(\gamma)$. Other backgrounds are not subtracted. For each of the energy bins, Table 3 shows the maximum and minimum limits obtained in the region of the (M_X, M_Y) plane described above. Fig. 2 shows the 95% CL lower limits on $\sigma(e^+e^- \to XX) \cdot BR^2(X \to Y\gamma)$ at $\sqrt{s} = 207$ GeV, obtained from all OPAL data with $\sqrt{s} \geqslant 189$ GeV, under the assumption that $\sigma(e^+e^- \to XX)$ scales with centre-of-mass energy as β_X/s. These limits range from 10–60 fb.

Systematic uncertainties arise from the sources described in Section 4. However, there are additional contributions due to limited Monte Carlo statistics at each of the generated (M_X, M_Y) points and from uncertainties on the efficiency parameterization across the (M_X, M_Y) plane and as a function of energy. The combined relative uncertainty on the efficiency varies from about 3% to 6% across the plane (for $M_X - M_Y > 5$ GeV). The uncertainty on the expected SM background contribution is 2.6%. In calculating the limits, systematic uncertainties are accounted for in the manner advocated in Ref. [22]. This also applies to the limits for the $M_Y \approx 0$ case, presented in the next section.

Table 3
Results of individual limit calculations at each centre-of-mass energy. The first column shows the data sample. The second and third columns show the maximum and minimum 95% CL limits on $\sigma(e^+e^- \to XX) \cdot BR^2(X \to Y\gamma)$ in the (M_X, M_Y) plane, for the case of massive Y for $M_X > M_Z/2$ and $M_X - M_Y < 5$ GeV. The last two columns show the minimum and maximum 95% CL limits obtained for the special case of $M_Y \approx 0$, for M_X values between 45 GeV and the kinematic limit

$\sqrt{s}$	$\sigma_{95}^{\min}(M_X, M_Y)$	$\sigma_{95}^{\max}(M_X, M_Y)$	$\sigma_{95}^{\min}(M_X)$	$\sigma_{95}^{\max}(M_X)$
192	138 fb	296 fb	143 fb	288 fb
196	60 fb	125 fb	71 fb	87 fb
200	57 fb	278 fb	57 fb	237 fb
202	105 fb	323 fb	106 fb	206 fb
205	52 fb	183 fb	70 fb	130 fb
207	31 fb	90 fb	45 fb	70 fb

5.2. *Search for* $e^+e^- \to XX$, $X \to Y\gamma$; *special case:* $M_Y \approx 0$

For the special case of $M_Y \approx 0$ the applied kinematic consistency requirements differ from those used for the general case. One can calculate [23] the maximum mass, $M_X^{\max}$, which is consistent with the measured three-momenta of the two photons, assuming a massless Y. A cut on $M_X^{\max}$ provides further suppression of the $\nu\bar{\nu}\gamma\gamma(\gamma)$ background while retaining high efficiency for the signal hypothesis. This is discussed in more detail in Ref. [3]. To allow for resolution effects, we require that the maximum kinematically al-

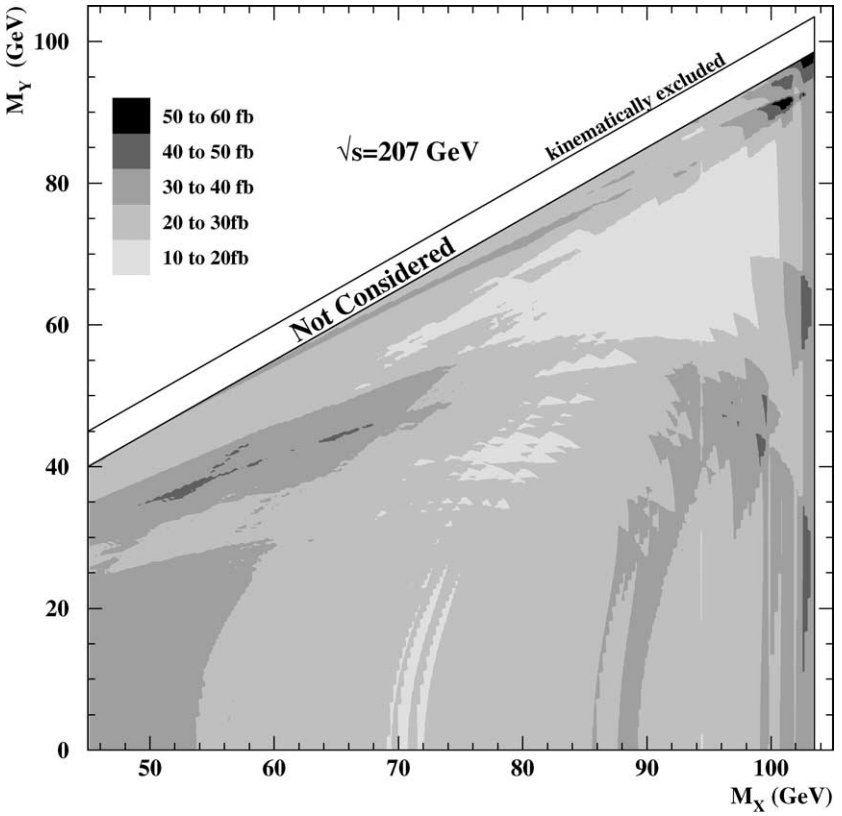

Fig. 2. The shaded areas show 95% CL upper limits on the quantity $\sigma(e^+e^- \to XX) \cdot BR^2(X \to Y\gamma)$ at $\sqrt{s} = 207$ GeV obtained from all OPAL data with $\sqrt{s} \geqslant 189$ GeV, under the assumption that the cross-section scales as β_X/s. No limit is set for mass-difference values $M_X - M_Y < 5$ GeV, defined by the lower line above the shaded regions. The upper line is for $M_X = M_Y$.

lowed mass be greater than $M_X - 5$ GeV. This has better than 96% relative efficiency for signal at all values of M_X while suppressing much of the remaining $\nu\bar{\nu}\gamma\gamma(\gamma)$ background.

The $M_X^{\max}$ distributions for all selected events, divided into the 192–202 GeV and 205–207 GeV data samples, are shown in Fig. 3. In each case, the points with error bars show the OPAL data while the unshaded histogram shows the expected contribution from the $e^+e^- \to \nu\bar{\nu}\gamma\gamma(\gamma)$, from KK2f Monte Carlo, normalized to the luminosity of the data. Shown as a shaded histogram in the 205–207 GeV plot is the expected distribution from signal Monte Carlo events generated with $M_X = 100$ GeV (with arbitrary normalization). For this $M_Y \approx 0$ case, the signal reconstruction efficiencies calculated from Monte Carlo events generated at $\sqrt{s} = 206$ GeV are shown in Table 4 after application of the event selection criteria and then after the cut on $M_X^{\max}$. Also shown in Table 4 are the numbers of events selected from the 205–207 GeV data sample which are consistent with each value of M_X as well as the expected number of $e^+e^- \to \nu\bar{\nu}\gamma\gamma(\gamma)$ events. The number of selected events (from the 205–207 GeV sample) consistent with a given value of M_X varies from 10, for $M_X \geqslant 45$ GeV, to 2 at the kinematic limit. The expected number of events decreases from 14.9 ± 0.4 at $M_X \geqslant 45$ GeV to 1.28 ± 0.08 consistent with $M_X \geqslant 102.5$ GeV.

Based on the efficiencies and the number of selected events, we calculate 95% CL upper limits on $\sigma(e^+e^- \to XX) \cdot BR^2(X \to Y\gamma)$ for $M_Y \approx 0$ as a function of M_X, in each region of centre-of-mass energy. The last two columns of Table 3 show the range of limits obtained from each of the data samples, for M_X values from 45 GeV up to the kinematic limit.

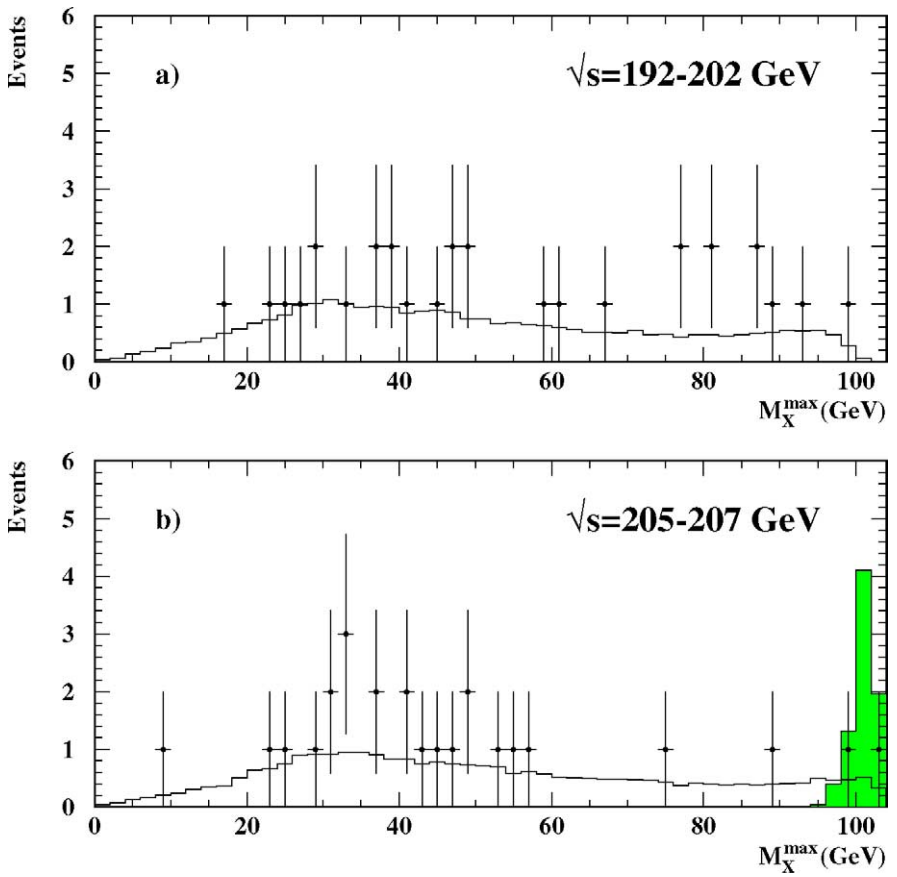

Fig. 3. The calculated value of $M_{\mathrm{X}}^{\max}$ for events selected from (a) the 192–202 GeV data sample and (b) the 205–207 GeV sample. In each case the data points show the OPAL data and the unshaded histogram shows the expected distribution from the Standard Model process $\mathrm{e}^+\mathrm{e}^- \to \nu\bar{\nu}\gamma\gamma(\gamma)$, evaluated using KK2f and normalized to the integrated luminosity of the data sample. In (b) the shaded histogram shows the expected distribution for the signal process $\mathrm{e}^+\mathrm{e}^- \to \mathrm{XX}$, $\mathrm{X} \to \mathrm{Y}\gamma$ for $M_{\mathrm{X}} = 100$ GeV with arbitrary production cross-section.

Table 4
Selection efficiencies as a function of M_{X} for the process $\mathrm{e}^+\mathrm{e}^- \to \mathrm{XX}$, $\mathrm{X} \to \mathrm{Y}\gamma$, for $M_{\mathrm{Y}} \approx 0$ at $\sqrt{s} = 206$ GeV. The second column shows the efficiency of the general selection. The third column shows the efficiency including the additional cut on $M_{\mathrm{X}}^{\max}$. The errors on the efficiencies are statistical only. The fourth column shows the number of events from the 205–207 GeV data sample consistent with the mass value M_{X}. The last column shows the corresponding number of expected events from the process $\mathrm{e}^+\mathrm{e}^- \to \nu\bar{\nu}\gamma\gamma(\gamma)$, obtained using KK2f, along with the corresponding uncertainty (statistical plus systematic)

M_{X} (GeV)	Selection efficiency (%)	Selection efficiency (%) with $M_{\mathrm{X}}^{\max} > M_{\mathrm{X}} - 5$ GeV	N_{data}	$N_{\nu\bar{\nu}\gamma\gamma(\gamma)}$
102.5	75.6 ± 1.1	73.6 ± 1.3	2	1.28 ± 0.08
100	75.7 ± 1.1	72.7 ± 1.3	2	2.08 ± 0.10
90	74.9 ± 1.1	72.5 ± 1.2	3	4.14 ± 0.16
80	73.7 ± 1.2	71.3 ± 1.2	4	6.13 ± 0.22
70	74.5 ± 1.2	71.7 ± 1.2	5	8.51 ± 0.28
60	73.9 ± 1.2	72.2 ± 1.2	5	11.25 ± 0.34
50	72.3 ± 1.2	69.5 ± 1.2	10	14.85 ± 0.42

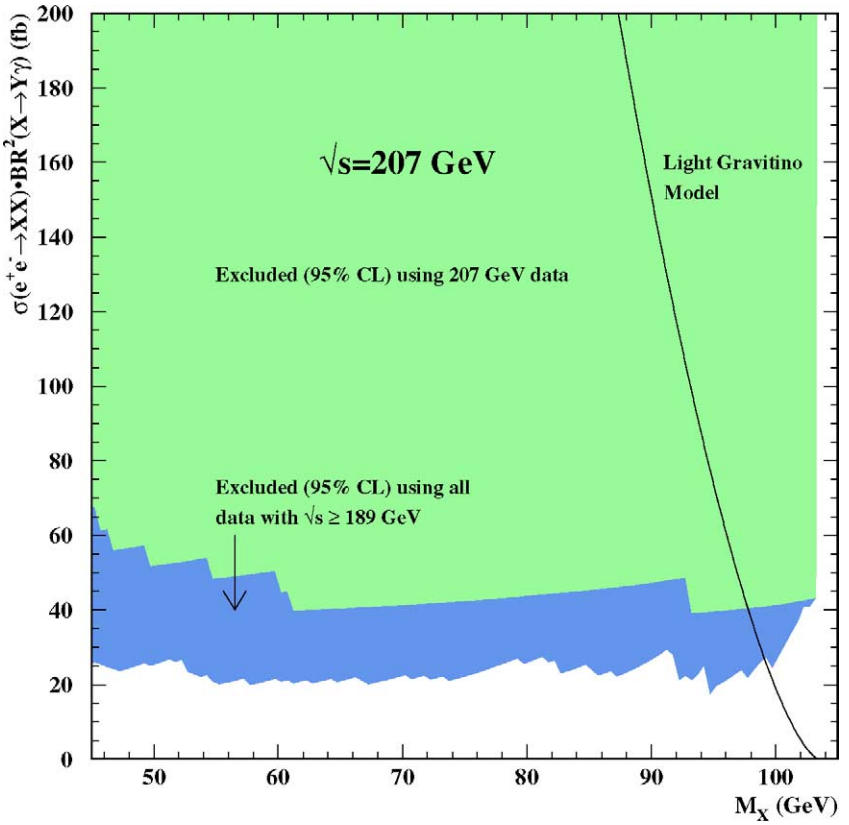

Fig. 4. 95% CL upper limits on $\sigma(e^+e^- \to XX) \cdot BR^2(X \to Y\gamma)$ at 207 GeV for $M_Y \approx 0$ obtained from all OPAL data with $\sqrt{s} \geqslant 189$ GeV. The lightly shaded region shows the excluded region obtained using only the OPAL 207 GeV data sample. The darker region shows the exclusion region obtained using all OPAL data with $\sqrt{s} \geqslant 189$ GeV, assuming that the cross-section scales as β_X/s. The line shows the prediction of an example light gravitino LSP model [5]. Within that model, $\tilde{\chi}_1^0$ masses between 45 and 99 GeV are excluded at 95% CL. These limits assume that particle X decays promptly.

Fig. 4 shows the limit obtained from the 207 GeV data sample, as well as the combined limit obtained from the entire data sample with $\sqrt{s} \geqslant 189$ GeV assuming that the cross-section scales as β_X/s. For the mass range of interest ($M_X > 45$ GeV) the model-independent limits range between 45 and 70 fb while the combined limits range between 20 and 45 GeV. These limits[25] can be used to set model-dependent limits on the mass of the lightest neutralino in supersymmetric models in which the NLSP is the lightest neutralino and the LSP is a light gravitino ($X = \tilde{\chi}_1^0, Y = \tilde{G}$). Shown in Fig. 4, as a dotted line, is the (Born-level) cross-section prediction from a specific light gravitino LSP model [5] in which the neutralino composition is purely bino, with $m_{\tilde{e}_R} = 1.35 m_{\tilde{\chi}_1^0}$ and $m_{\tilde{e}_L} = 2.7 m_{\tilde{\chi}_1^0}$. Within the framework of this model, $\tilde{\chi}_1^0$ masses between 45 and 99.0 GeV are excluded at 95% CL.

As described in Section 2, the efficiencies over the full angular range have been obtained using isotropic angular distributions for the production and decay of X. The validity of this model has been examined based on the angular distributions calculated for photino pair production in Ref. [24]. For models proposed in Ref. [25], the production angular distributions

[25] In the 70–80 GeV region the limits are actually slightly worse than those along the $M_Y = 0$ axis of Fig. 2 despite the more efficient background suppression of the $M_X^{\max}$ cut, relative to the kinematic consistency cuts applied in the general case. This is due to a deficit of selected events in this region, compared to the expected background when using the general kinematic consistency requirements.

are more central and so this procedure is conservative. For a $1 + \cos^2\theta$ production angular distribution expected for t-channel exchange of a very heavy particle according to Ref. [24], the relative efficiency reduction would be less than 2% at all points in the (M_X, M_Y) plane.

6. Conclusions

We have searched for events with a final state consisting of two or three photons and large missing energy, in data taken with the OPAL detector at LEP, at centre-of-mass energies in the range of 192–209 GeV. The 54 events observed in the data are consistent with the expectations of 57.2 ± 1.3 events from the Standard Model process $e^+e^- \to \nu\bar{\nu}\gamma\gamma(\gamma)$ and 1.2 ± 0.3 events from other Standard Model and background sources. The number of events observed in the data and their kinematic distributions are consistent with Standard Model expectations. Limits on new physics processes of the form $\sigma(e^+e^- \to XX) \cdot BR^2(X \to Y\gamma)$ are set separately at energies of 192, 196, 200, 202, 205 and 207 GeV. In addition, combined limits are set at $\sqrt{s} = 207$ GeV, assuming a β_X/s scaling of the production cross-section $\sigma(e^+e^- \to XX)$. From the full OPAL data sample with $\sqrt{s} \geqslant 189$ GeV, we derive 95% CL upper limits on $\sigma(e^+e^- \to XX) \cdot BR^2(X \to Y\gamma)$ ranging from 10 to 60 fb for the general case of massive X and Y. For the special case of $M_Y \approx 0$, the 95% CL upper limits on $\sigma(e^+e^- \to XX) \cdot BR^2(X \to Y\gamma)$ range from 20 to 45 fb, for $M_X > 45$ GeV. These results are used to place model-dependent lower limits on the $\tilde{\chi}_1^0$ mass in a specific light gravitino LSP model [5]. Masses between 45 and 99 GeV are excluded at 95% CL. All limits assume that particle X decays promptly.

Acknowledgements

We particularly wish to thank the SL Division for the efficient operation of the LEP accelerator at all energies and for their close cooperation with our experimental group. In addition to the support staff at our own institutions we are pleased to acknowledge the

- Department of Energy, USA,
- National Science Foundation, USA,
- Particle Physics and Astronomy Research Council, UK,
- Natural Sciences and Engineering Research Council, Canada,
- Israel Science Foundation, administered by the Israel Academy of Science and Humanities,
- Benoziyo Center for High Energy Physics,
- Japanese Ministry of Education, Culture, Sports, Science and Technology (MEXT) and a grant under the MEXT International Science Research Program,
- Japanese Society for the Promotion of Science (JSPS),
- German Israeli Bi-national Science Foundation (GIF),
- Bundesministerium für Bildung und Forschung, Germany,
- National Research Council of Canada,
- Hungarian Foundation for Scientific Research, OTKA T-038240, and T-042864,
- The NWO/NATO Fund for Scientific Research, the Netherlands.

References

[1] OPAL Collaboration, G. Abbiendi, et al., Eur. Phys. J. C 18 (2000) 253.
[2] OPAL Collaboration, G. Abbiendi, et al., Eur. Phys. J. C 8 (1999) 23.
[3] OPAL Collaboration, K. Ackerstaff, et al., Eur. Phys. J. C 2 (1998) 607.
[4] ALEPH Collaboration, A. Heister, et al., Eur. Phys. J. C 28 (2003) 1;
DELPHI Collaboration, J. Abdallah, et al., CERN-EP-2003-093, Eur. Phys. J., submitted for publication;
L3 Collaboration, P. Achard, et al., Phys. Lett. B 587 (2004) 16.
[5] C.Y. Chang, G.A. Snow, UMD/PP/97-57;
K.S. Babu, C.F. Kolda, F. Wilczek, Phys. Rev. Lett. 77 (1996) 3070.
[6] OPAL Collaboration, G. Abbiendi, et al., Phys. Lett. B 544 (2002) 44.
[7] OPAL Collaboration, G. Abbiendi, et al., CERN-EP-2004-003, Phys. Rev. D, submitted for publication.
[8] OPAL Collaboration, K. Ahmet, et al., Nucl. Instrum. Methods A 305 (1991) 275;
S. Anderson, et al., Nucl. Instrum. Methods A 403 (1998) 326;
B.E. Anderson, et al., IEEE Trans. Nucl. Sci. 41 (1994) 845.
[9] G. Montagna, M. Moretti, O. Nicrosini, F. Piccinini, Nucl. Phys. B 541 (1999) 31.
[10] S. Jadach, B.F.L. Ward, Z. Wąs, Phys. Lett. B 449 (1999) 97;

S. Jadach, B.F.L. Ward, Z. Wąs, Comput. Phys. Commun. 130 (2000) 260.
[11] F.A. Berends, R. Kleiss, Nucl. Phys. B 186 (1981) 22.
[12] S. Jadach, W. Placzek, B.F.L. Ward, Phys. Lett. B 390 (1997) 298.
[13] D. Karlen, Nucl. Phys. B 289 (1987) 23.
[14] S. Jadach, et al., Comput. Phys. Commun. 119 (1999) 272.
[15] J. Fujimoto, et al., Comput. Phys. Commun. 100 (1997) 128.
[16] S. Jadach, B.F.L. Ward, Z. Wąs, Comput. Phys. Commun. 79 (1994) 503;
Version 4.02 was used including a recommended correction to the NDIST0 subroutine.
[17] F.A. Berends, P.H. Daverveldt, R. Kleiss, Nucl. Phys. B 253 (1985) 421;
F.A. Berends, P.H. Daverveldt, R. Kleiss, Comput. Phys. Commun. 40 (1986) 271;
F.A. Berends, P.H. Daverveldt, R. Kleiss, Comput. Phys. Commun. 40 (1986) 285;
F.A. Berends, P.H. Daverveldt, R. Kleiss, Comput. Phys. Commun. 40 (1986) 309.
[18] J.A.M. Vermaseren, Nucl. Phys. B 229 (1983) 347.
[19] S. Katsanevas, S. Melachronios, Comput. Phys. Commun. 112 (1998) 227.
[20] J. Allison, et al., Nucl. Instrum. Methods A 317 (1992) 47.
[21] OPAL Collaboration, M.Z. Akrawy, et al., Phys. Lett. B 248 (1990) 211;
ALEPH Collaboration, D. Decamp, et al., Phys. Rep. 216 (1992) 253;
L3 Collaboration, M. Acciarri, et al., Phys. Lett. B 350 (1995) 109.
[22] R.D. Cousins, V.L. Highland, Nucl. Instrum. Methods A 320 (1992) 331.
[23] J.L. Lopez, D.V. Nanopoulos, Phys. Rev. D 55 (1997) 4450.
[24] J. Ellis, J.S. Hagelin, Phys. Lett. B 122 (1983) 303.
[25] S. Dimopoulos, et al., Phys. Rev. Lett. 76 (1996) 3494;
D.R. Stump, M. Wiest, C.P. Yuan, Phys. Rev. D 54 (1996) 1936;
S. Ambrosanio, et al., Phys. Rev. D 54 (1996) 5395.